

Title	A study on the spatial dependence of a MEMS electromagnetic transducer
Authors	Houlihan, Ruth;Jackson, Nathan;Mathewson, Alan;Olszewski, Oskar Zbigniew
Publication date	2019-01-10
Original Citation	Houlihan, R., Jackson, N., Mathewson, A. and Olszewski, O. Z. (2019) 'A Study on the Spatial Dependence of a MEMS Electromagnetic Transducer', Journal of Microelectromechanical Systems, 28(2), pp. 290-297. doi: 10.1109/JMEMS.2018.2887004
Type of publication	Article (peer-reviewed)
Link to publisher's version	<a href="https://ieeexplore.ieee.org/document/8607961">https://ieeexplore.ieee.org/document/8607961</a> - 10.1109/JMEMS.2018.2887004
Rights	© 2019 IEEE. Personal use of this material is permitted. Permission from IEEE must be obtained for all other uses, in any current or future media, including reprinting/republishing this material for advertising or promotional purposes, creating new collective works, for resale or redistribution to servers or lists, or reuse of any copyrighted component of this work in other works.
Download date	2023-05-05 21:04:17
Item downloaded from	<a href="http://hdl.handle.net/10468/7762">http://hdl.handle.net/10468/7762</a>



# UCC

**University College Cork, Ireland**  
Coláiste na hOllscoile Corcaigh

# A Study on the Spatial Dependence of a MEMS Electromagnetic Transducer

Ruth Houlihan<sup>1</sup>, Nathan Jackson, *Senior Member, IEEE*, Alan Mathewson, *Senior Member, IEEE*, and Oskar Z. Olszewski<sup>2</sup>

**Abstract**—A MEMS, silicon-based device with a piezoelectric layer and an integrated magnet is presented for magnetic to electrical transduction. The cantilever structure can be configured either as an energy harvester to harvest power from an AC power line or as an AC current sensor. The positioning of the transducer with respect to the conductor is critical in both scenarios. For the energy scavenger, correct positioning is required to optimize the harvested power. For the current sensor, it is necessary to optimize the sensitivity of the sensor. This paper considers the effect of the relative position of the transducer with respect to the wire on the resulting electromagnetic forces and torques driving the device. It is shown in this paper that it is the net equivalent torque at the anchor that must be considered and not just the vertical component of the magnetic force as has been widely assumed heretofore. We show that for single wire conductors, the commonly made assumption that there exists two symmetrical power peaks at 45° either side of the wire is untrue, but rather that the net driving torque on one side of the wire can be more than an order of magnitude greater than the other. [2018-0173]

**Index Terms**—Energy harvesting, Piezoelectric transducers, Electromagnetic analysis, Electromagnetic forces, Mechanical vibrations, Torque.

## I. INTRODUCTION

ONE approach towards the transduction of AC electromagnetic energy uses a permanent magnet on a moveable mechanical element such as a cantilever. The alternating electromagnetic field exerts an alternating force on the magnet that in turn drives the cantilever into oscillation at the frequency of the source. A piezoelectric layer deposited on the cantilever can be used to transduce strain in the cantilever resulting from the oscillations. The arrangement has been described in the literature both for energy harvesting [1], [8], [10], [11], [13] and current sensing applications [5], [7], [12], [15] and is shown schematically in Figure 1. As an energy harvester, the approach has the advantage that the source frequency is very well defined and so the challenge of designing an inherently narrow bandwidth harvester with

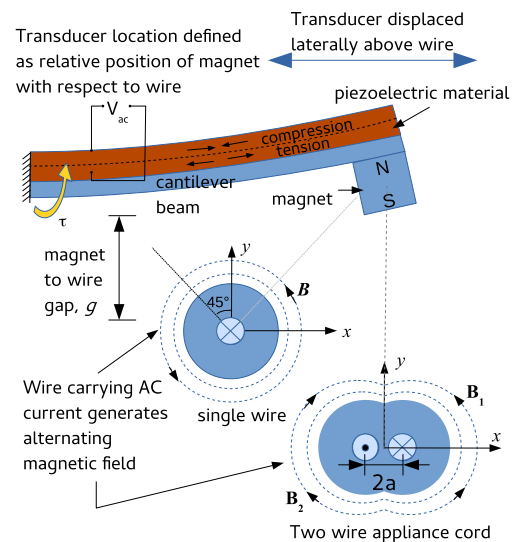


Fig. 1. Schematic showing piezo-magnetic transducer concept. As the cantilever beam is moved laterally above the wire, the torque at the beam anchor resulting from the interaction between the wire's magnetic field and the magnet varies significantly.

an ill-defined or broadband vibration source is averted. As a current sensing device, the piezoelectric beam with an integrated magnet is passive, non-invasive and does not require cord separation.

The positioning of the MEMS transducer is critical in both the harvester and sensor applications, as it defines the electromagnetic forces and torques acting on the cantilever magnet and thereby indirectly determines the power available for harvesting and/or the sensitivity of the sensor. This paper presents the theory describing the driving forces and torques that act on a magnet in an alternating electromagnetic field. This effect has been considered by the various groups that have published in this field. In particular, initial work done by Leland [6], [7], [9] and Paprotny [13] found in the analyses of the forces on a permanent magnet near an AC current-carrying wire, that only the vertical component of the force, which is proportional to the gradient of the electromagnetic field, needed to be accounted for (assuming magnetisation of the magnet is in the vertical ( $y$ ) direction). For a single wire conductor, this assumption results in the maximum force occurring at a 45° offset to the vertical; for a two wire zip-cord it occurs directly in line with the cord's vertical ( $y$ ) axis (refer to Figure 1). Subsequent work tended to adopt this

Manuscript received July 27, 2018; revised November 14, 2018; accepted December 8, 2018. Subject Editor L. Buchailot. This work was supported by Enterprise Ireland. (Corresponding author: Ruth Houlihan.)

R. Houlihan and O. Z. Olszewski are with the Tyndall National Institute, T12 RSCP Cork, Ireland (e-mail: ruth.houlihan@tyndall.ie).

N. Jackson is with the Mechanical Engineering Department, The University of New Mexico, Albuquerque, NM 87131 USA (e-mail: njack@unm.edu).

A. Mathewson, retired, was with the Tyndall National Institute, T12 RSCP Cork, Ireland (e-mail: alan.mathewson@tyndall.ie).

Color versions of one or more of the figures in this paper are available online at <http://ieeexplore.ieee.org>.

Digital Object Identifier 10.1109/JMEMS.2018.2887004

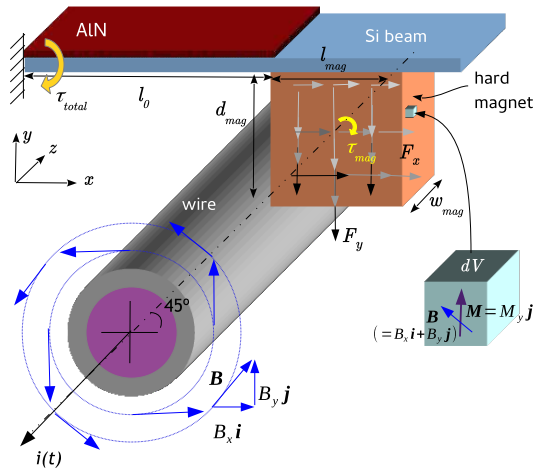


Fig. 2. Schematic showing the lateral and vertical forces acting on a cantilever magnet that is in close proximity to a current carrying conductor. In the arrangement shown, the magnet is positioned along the 45° axis relative to the wire's vertical axis.

hypothesis: Isagawa [3], Suzuki [14] and Xu [20] for example, also assumed the optimal force to occur along a 45° line to the magnet axis, although measurement results on a two-wire zip cord were poorly matched to the theory [16], [18] and much effort was made into addressing the disparity with a positional correction scheme [17], [19].

In reality, an electromagnetic transducer in the form of a cantilever beam with an integrated magnet is driven by a combination of torque components and the omission, in particular, of the magnetic torque, has rendered previous studies inaccurate. In this work, all of the torque components driving the harvester are considered and the effect of their omission on both single wire and two-wire cords are considered. An analytical treatment of the problem compares the sum of the torque components with the spatial dependence of the transducer relative to the wire. It shows that the maximum force on the transducer depends on the magnet dimensions, its position on the cantilever and the gap between the magnet and the wire. The results are compared with measurements and show excellent agreement.

## II. THEORETICAL BACKGROUND

Consider a piezoelectric cantilever, oriented such that the beam length is normal to a conductor carrying an alternating current Figure 2. The axis of the conductor is designated the  $z$ -axis. The beam length is aligned with the  $x$ -axis and its thickness with the  $y$ -axis. A permanent magnet, magnetized along the  $y$ -axis, with remanence  $\mathbf{M} = M_y \mathbf{j}$ , and positioned near the cantilever tip experiences alternating electromagnetic forces that will cause the cantilever to oscillate with the same frequency as the AC signal in the wire. If the cantilever is designed such that this frequency matches its natural resonance, then mechanical amplification of the electromagnetic response will occur. A piezoelectric film disposed on the beam can then be used to convert the mechanical oscillations into an electrical output signal either for harvesting and/or sensing. Figure 2 shows the  $x$ -axis and  $y$ -axis forces ( $F_x$  and  $F_y$  respectively) that act on a magnet positioned on a cantilever beam and in close proximity to a magnetic field source. If it is

considered that it is torque rather than force that drives the electromagnetic transducer then it is the net torque acting at the beam anchor,  $\tau_{total}$ , that is of interest when determining the cantilever response.  $\tau_{total}$  is given by Equation 1.

$$\tau_{total} = \tau(F_x) + \tau(F_y) + \tau'_{mag} \quad (1a)$$

$$= \int_{l_0}^{l_0+l_{mag}} F_y dx + \int_{-d_{mag}}^0 F_x dy + \tau'_{mag} \quad (1b)$$

where  $\tau(F_x)$  is the torque at the beam anchor resulting from the lateral magnetic force  $F_x$ ;  $\tau(F_y)$  is the torque resulting from the vertical magnetic force  $F_y$ ; and  $\tau'_{mag}$  is the equivalent torque at the beam anchor resulting from the magnetic torque on the magnet in an electromagnetic field. Note that the magnetic torque,  $\tau_{mag}$ , acts through the center of the magnet but can be resolved into a pair of opposing lateral forces that act at the top and bottom of the magnet. This equivalent force couple can then be converted back into an equivalent torque at the anchor. In the instance where the beam thickness is negligible relative to the magnet thickness,  $\tau'_{mag} \sim \tau_{mag}$ .

As mentioned in Section I, prior work in this area analyzed the response of the beam to the vertical force component,  $F_y$ , only. The contribution of the lateral force,  $F_x$ , was considered negligible and for thin magnets (less than  $\sim 1$  mm thick), this is indeed the case. The contribution of the magnetic torque,  $\tau_{mag}$ , has not been considered previously. In the following, each of these torque components in Equation 1 is individually addressed and their impact on the mechanical response of the cantilever determined.

The net force on a magnetic dipole moment in a non-uniform magnetic field,  $\mathbf{F}_p$ , is given by [4, eq. (2)].

$$\mathbf{F}_p = (\mathbf{p} \cdot \nabla) \mathbf{B} = \nabla(\mathbf{p} \cdot \mathbf{B}) \quad (2)$$

where  $\mathbf{p}$  is the dipole moment and  $\mathbf{B}$  is the magnetic field vector. A permanent magnet of volume,  $V$ , and with remanence,  $\mathbf{M}$ , can be considered to have an associated dipole moment,  $\mathbf{p}_M$ , where  $\mathbf{p}_M = \int \mathbf{M} dV$  and so the total force on a permanent magnet in a non-uniform electromagnetic field can be expressed by Equation 2 with  $\mathbf{p} \rightarrow \mathbf{p}_M$ .

$$\mathbf{F}_{mag} (= F_x \mathbf{i} + F_y \mathbf{j} + F_z \mathbf{k}) = \int_V \nabla (\mathbf{M} \cdot \mathbf{B}) dV \quad (3)$$

If the source of the electromagnetic field is a very long, current carrying conductor aligned with the  $z$ -axis, then the magnitude of the field at any point has a spatial dependence only on  $\mathbf{r}$ , where  $\mathbf{r} = x \mathbf{i} + y \mathbf{j}$ , the radial distance between the wire and the point. Considering that our magnet is magnetized in the  $y$ -direction only ( $\mathbf{M} = M_y \mathbf{j}$ ), Equation 3 reduces to

$$\mathbf{F}_{mag} = w_{mag} \int_A \left[ M_y \frac{\partial B_y}{\partial x} \right] \mathbf{i} + \left[ M_y \frac{\partial B_y}{\partial y} \right] \mathbf{j} dA \quad (4)$$

where  $w_{mag}$  is the magnet dimension in the  $z$ -direction,  $B_x$  and  $B_y$  are the horizontal and vertical components of the magnetic field vector  $\mathbf{B}$  respectively, and  $A$  is the area of the magnet in the  $x$ - $y$  plane.

It is clear from Equation 4 that the magnet experiences force contributions in both the lateral and the vertical directions. These forces,  $F_x$  and  $F_y$ , are proportional to the gradient of

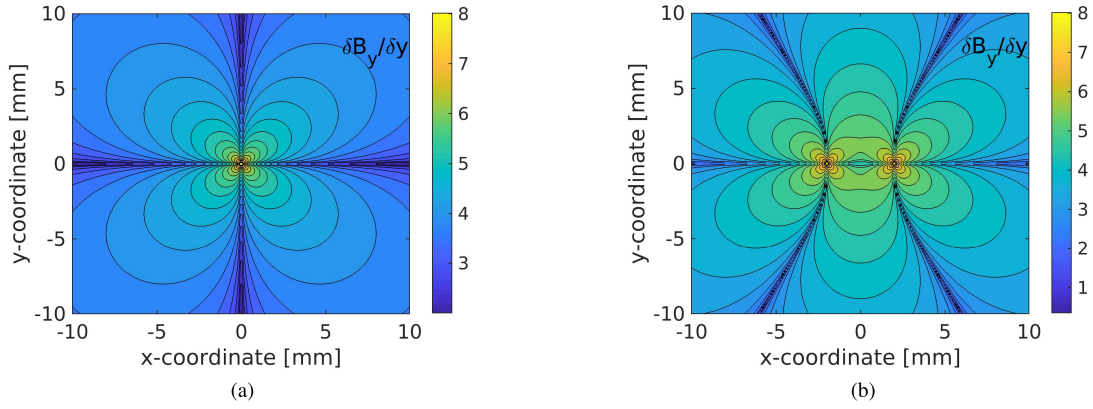


Fig. 3. Contour plot showing the log of the gradient of  $B_y$  with respect to  $y$ ,  $\log(\partial B_y/\partial y)$ , around a single wire power cord and a two-wire power cord. The vertical component of the electromagnetic force,  $F_y$  is directly proportional to  $\partial B_y/\partial y$ . The colorbar indicates the power  $n$ , where  $10^n = |\partial B_y/\partial y|$  and so the higher field gradients are shown by white/yellow and the lowest field gradients by the dark blue. (a) single wire cord. (b) two-wire cord.

the  $y$ -component of the magnetic field,  $B_y$ , with respect to their respective axes. The magnitude of the magnetic field at a radial distance  $r$  from a current carrying wire can be calculated using Ampère's law which, when simplified for a long, straight wire, is given as

$$B = \frac{\mu_0 I}{2\pi r} = \frac{\mu_0 I}{2\pi \sqrt{x^2 + y^2}} \quad (5)$$

where  $\mu_0$  is the permeability of free space and  $I$  is the current in the wire. The gradient of the  $y$ -component of the field,  $\partial B_y/\partial y$  is then given by Equation 6 for a single wire power cord.

$$\frac{\partial B_y}{\partial y} = \frac{\mu_0 I}{2\pi} \frac{-2xy}{(x^2 + y^2)^2} \quad (6)$$

For a two-wire cord (zip-wire), the contribution of the fields from both wires are combined according to Equation 7, where  $2a$  is the distance between the individual wires in the power cable (see Figure 1).

$$\frac{\partial B_y}{\partial y}^{2\text{wire}} = \frac{\mu_0 I}{2\pi} \left[ \frac{-2(x+a)y}{((x+a)^2 + y^2)^2} + \frac{2(x-a)y}{((x-a)^2 + y^2)^2} \right] \quad (7)$$

The field gradient is shown in a contour plot in Figure 3(a) for a single wire power cord and in Figure 3(b) for a two-wire power cord. The figures, which plot the spatial distribution of the logarithm (for ease of visualization) of the field gradient i.e.  $\log(|\partial B_y/\partial y|)$ , were created using Matlab. The plot of  $\partial B_y/\partial x$  is simply a rotation by  $45^\circ$  of the  $\partial B_y/\partial y$  plot.

It seems, from Figure 3(a), that in order to optimize the vertical component of the magnetic force (and subsequently the torque resulting from that force,  $\tau(F_y)$ ) for a single wire cord, the magnet should be positioned at  $45^\circ$  to the wire and indeed, this is the observation made previously in the literature [7], [20]. Similarly, for a two-wire cable it would seem that the optimal position for the transducer is directly above the wire and again, this is the approach proffered in the literature [6]. The  $x$ -component of the force acting on the magnet,  $F_x$ , is in most instances justifiably neglected since typically  $\tau(F_x) \ll \tau(F_y)$  except where a very thick magnet is used and/or the magnet is positioned very close to the beam anchor [2].

The force described by Equation 4 is the force on a magnet in a non-uniform electromagnetic field. There are, however, an additional pair of forces acting on the magnet, not accounted for by Equation 4, which act in a uniform field and tend to rotate the magnet into the field. The torque resulting from these forces acts about the center of the magnet and is given by Equation 8.

$$\tau_{\text{mag}} = \int_v \mathbf{M} \times \mathbf{B} \, dV \quad (8)$$

Unlike the  $\tau(F_x)$ , the magnetic torque  $\tau_{\text{mag}}$  is comparable in magnitude to the torque generated by the vertical forces  $\tau(F_y)$  and cannot be omitted from calculations. For the two-dimensional system described and assuming that the magnet is polarised in the  $y$ -direction only, Equation 8 reduces to

$$\tau_{\text{mag}} = \int_v M_y \cdot B_x \, dV \quad (9)$$

The magnetic torque therefore is directly proportional to the magnetic field component  $B_x$ , which is plotted in Figure 4(a) for a single wire cord and in Figure 4(b) for a two-wire cord. As evident from the figures,  $B_x$  and consequently,  $\tau_{\text{mag}}$ , is maximized when the magnet is positioned directly over the wire in the case of the single wire cord, and at  $45^\circ$  in the case of a two-wire cord.

### III. MODELING RESULTS

Each of the three individual torque components that contribute to the displacement of the cantilever have a spatial dependence and their respective magnitudes varies as the magnet is moved horizontally above the wire. In Figure 5(a)-(d), the contribution of the different torque components acting on a 10 mm long, 50  $\mu\text{m}$  thick silicon cantilever versus axial position are shown for various magnet configurations. Calculations were performed in Matlab.

In all instances, the vertical component of the magnetic force,  $\tau(F_y)$ , is zero directly above the wire and increases to its maximum value as the magnet approaches the  $45^\circ$  axes either side of the vertical ( $y$ ) axis. The direction of the vertical force switches as the magnet passes the  $y$  axis. By comparison, the horizontal component of the force,  $\tau(F_x)$ , and the magnetic

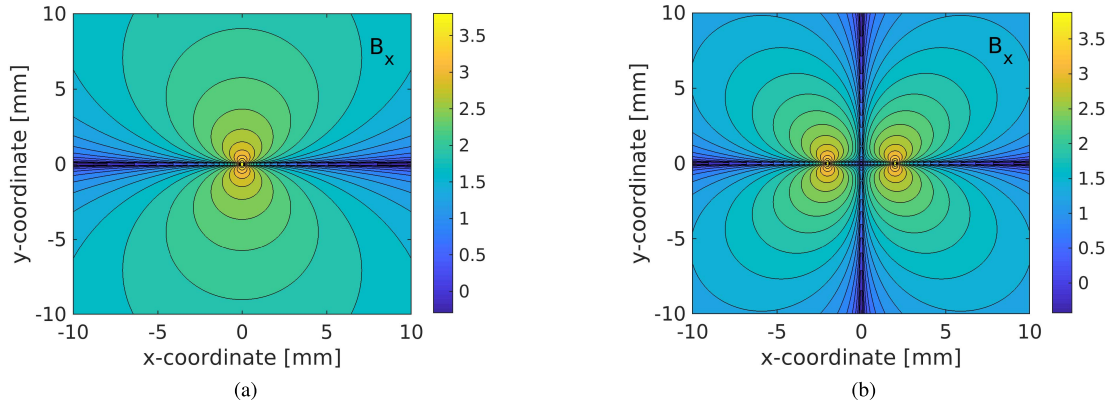


Fig. 4. Contour plot showing the logarithm of the magnetic field component,  $B_x$  for (a) a single wire power cord and (b) a two-wire power cord. The magnetic torque,  $\tau_{mag}$  is directly proportional to  $B_x$  according to Equation 9. The colorbar indicates the power  $n$ , where  $10^n = |B_x|$  and so the higher field gradients are shown by white/yellow and the lowest field gradients by the dark blue.

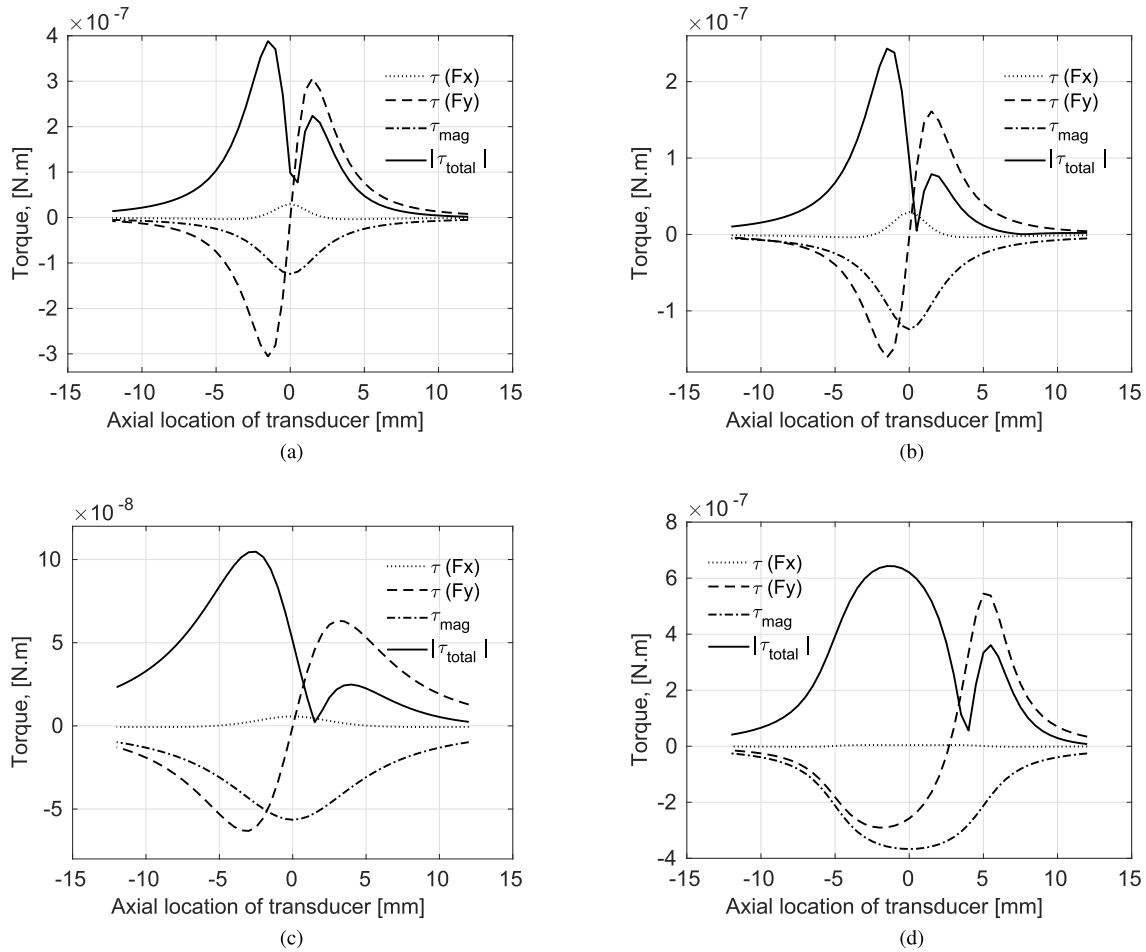


Fig. 5. Graphs illustrate how the torque at the anchor of a cantilever versus axial position varies depending on the cantilever configuration and the distance between the magnet and the wire,  $g$ . A cantilever of length 10 mm and thickness  $50 \mu\text{m}$  and a current of 1.5 A was assumed for the calculations. (a) 1 mm cube magnet at beam tip,  $g = 2$  mm. (b) 1 mm cube magnet midway along beam,  $g = 2$  mm. (c) 1 mm cube magnet at beam tip,  $g = 5$  mm. (d)  $100 \mu\text{m}$  thick magnet deposited over full beam,  $g = 2$  mm.

torque,  $\tau_{mag}$ , are both at a maximum when the magnet is directly above the wire and the direction of these stays the same as the magnet passes over the wire. The sum of the three torque components, denoted  $\tau_{total}$ , is notably different for the four cases considered. In Figure 5(a)-(b), a 1 mm cube

magnet and a 2 mm wire to magnet gap,  $g$ , is assumed with the difference in the graphs relating to the location of the magnet on the beam: in (a) it is assumed to sit at the tip of the cantilever whereas in (b) it is positioned mid-way along the beam. When positioned at the beam tip,  $\tau(F_y)$  is much



greater than  $\tau_{mag}$  and so the difference between the peaks that represent the optimal transducer location is less compared with (b) where  $|\tau_{mag}| \simeq |\tau(F_y)|$ . In Figure 5(c) a 5 mm gap between the wire and the transducer is assumed. Compared with (a) which has the same beam-magnet configuration,  $\tau_{mag}$  here is closer in magnitude to  $\tau(F_y)$ . This is because while  $\tau_{mag}$  is directly proportional to the magnetic field strength,  $\tau(F_y)$  is proportional to the gradient of field and so  $\tau(F_y)$  decays more rapidly with increasing distance from the wire than  $T_{mag}$ . Similarly to (b) the result here is significant asymmetry in the peaks. In Figure 5(d), we assume that a magnetic thin film has been deposited over the entire length of the cantilever. The most notable difference here compared with the results for the 1 mm cube magnet is the asymmetry in  $F(y)$ . This can be explained by considering the case when the center of the beam/magnet is directly over the wire. While the vertical forces acting on the magnet are identical either side of the wire, the forces at the tip of the beam have a much greater contribution to the torque  $\tau(F_y)$  than the forces acting closer to the anchor. The effect on  $\tau_{total}$  is a significant broadening of the dominant peak.

The difference in the results for the various magnet configurations serves to demonstrate that there is no universal rule regarding the optimal positioning of the transducer but rather that it is dependent on the magnet dimensions and on its position on the cantilever. Ideally, the spatial dependence of the transducer should be minimal allowing for greater ease of use and reduced error associated with implementation. The result in Figure 5(d) is of particular interest, because it infers that careful design of the cantilever and/or of the magnet could result in a transducer with a wider, flatter response curve and so would have less of a requirement for precision positioning and calibration. This may be of particular interest where magnetic material is deposited and so magnets of arbitrary shape can be realized. We suggest, for example, that a magnet with a trapezoidal plan view, where the widest end of the trapezoid is at the anchor and the narrowest at the tip, could result in a flatter peak since the  $\partial B_y / \partial y$  function which goes from a minimum directly above the wire to a maximum at  $45^\circ$  to the wire would be then scaled by the (linearly) decreasing function  $w_{mag}(x)$ , where  $w_{mag}$  is the width of the magnet. A full computational analysis of alternative shaped magnets will be considered in future work.

#### IV. COMPARISON OF MODELED AND MEASURED RESULTS

In order to verify the theory, a MEMS cantilever fabricated from SOI (silicon-on-insulator), with an attached off-the-shelf magnet neodymium magnet was used. The cantilever was originally fabricated as a piezoelectric vibration energy harvester, wherein the device silicon (50  $\mu\text{m}$  thick) was used to define the beam and the bulk silicon (535  $\mu\text{m}$  thick) was used to define the mass of the harvester. A 100 nm thick titanium layer was deposited on the top side of the beam, followed by a 0.5  $\mu\text{m}$  thick Aluminium Nitride layer and then the top electrode was defined by a 100nm thick Aluminium layer. These thin films define the piezoelectric capacitor which converts strain in the beam to an electrical output. After the thin

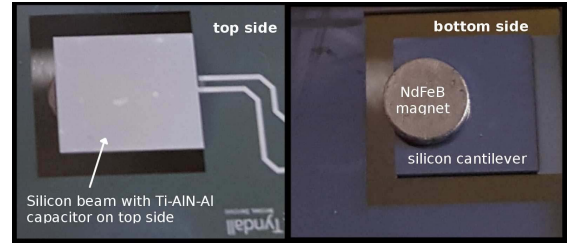


Fig. 6. Front and back sides of the MEMS harvester with attached magnet used here to validate theoretical results.

films were deposited, the lateral beam dimensions of the device were defined by a dry etch from the front side, and the mass was defined by a backside DRIE etch. Finally, the magnet was attached manually using a very thin layer of adhesive. Photos of the front and back sides of the harvester device are shown in Figure 6 and more complete details on the fabrication process is given in [11].

##### A. Single Wire Conductor

The results for a 50  $\mu\text{m}$  thick silicon cantilever with a 500  $\mu\text{m}$  thick mass with an attached magnet are shown for two different gap values in Figure 7. The magnet is a 500  $\mu\text{m}$  thick, 1 mm diameter, off-the-shelf neodymium disc magnet and is attached to the cantilever mass using epoxy as shown in the inset in Figure 7. The remanence of the magnet is 1.3 T. The assembled electromagnetic transducer was displaced laterally over a single electrical wire and the current in the piezoelectric capacitor was recorded. Lateral displacement of the transducer was achieved manually by sliding the PCB over a purpose machined perspex block through which holes for the wire were precision drilled at predetermined distances from the top surface. Lateral positioning was achieved simply using a scale ruler and measurements recorded at 1 mm intervals. An alternating current of 1.5 A with a frequency matching the resonance frequency of the cantilever (525 Hz), was generated using a custom built AC current source. The resistor used was 62 k $\Omega$ , chosen to match the impedance of the piezoelectric capacitor. The current generated in the capacitor was monitored as the cantilever was displaced laterally from one side of the wire to the other. The results are compared with the analytical model for gaps of 2.85 mm and 4.35 mm in Figure 7. The graphs show (i) very good agreement between the analytical and experimental results and (ii) while there are two peaks, they are highly asymmetrical confirming the result from our analytical study, that the magnetic torque cannot be omitted from calculations (consideration of  $(F_y)$  only would have resulted in two perfectly symmetrical peaks with a minimum at  $x = 0$ ).

##### B. Two-Wire Conductor

We also consider the spatial dependence of the piezo-magnetic transducer relative to a zip-cord (two-wire cable). The inclusion of the magnetic torque in the analysis of an electromagnetic transducer has slightly less impact when the source of the electromagnetic field is a two-wire cord since a minimum of the  $x$  component of the field,  $B_x$  (Figure 4(b))

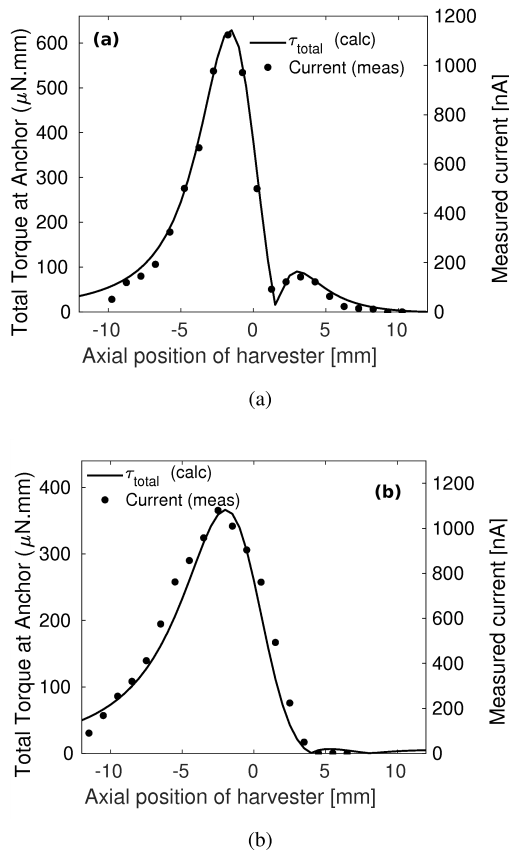


Fig. 7.  $\tau_{total}$  and measured current versus the relative position of the transducer compared with the wire for gaps of (a) 2.85 mm and (b) 4.35 mm.

coincides with the maximum of the field gradient,  $\partial B_y / \partial y$  (Figure 3(b)) and so the optimum position for the harvester remains directly over the wire. Nonetheless, the inclusion of the magnetic torque can be a significant contributor to  $\tau_{total}$ , the total torque at the anchor. To illustrate this, we consider the result published by Wang [16] and shown in Figure 8(a), which plots the measured voltage across the piezoelectric capacitor on a MEMS cantilever-type current sensor with a  $1 \text{ mm}^3$  magnet attached at the free end. Wang expected the experimental result to match his theoretical result which assumed that  $F_y$  is the only significant contributor to  $\tau_{total}$ . Instead of observing a major peak when the magnet is directly above the wire with two lesser side peaks (as suggested by the contour plot shown in Figure 3(b) and shown in the Figure 8(a) by the solid line), he measured three peaks of almost equal magnitude. He attributed the discrepancy between measurement and theory to experimental uncertainty regarding the ‘position and pose’ of the transducer relative to the wire. Figure 8(b) compares the torque at the anchor of the transducer resulting from the  $F_y$  alone to the total torque,  $\tau_{total}$  according to Equation 1. Beam and magnet dimensions were taken from Wang’s paper [15]. The analytic result for  $\tau_{total}$  in Figure 8(b) is an excellent match with Wang’s measured results.

### C. Irregular Magnet Shapes

It should be noted that the results in Figure 7 for a single wire and in Figure 8(b) for a two-wire cable are very

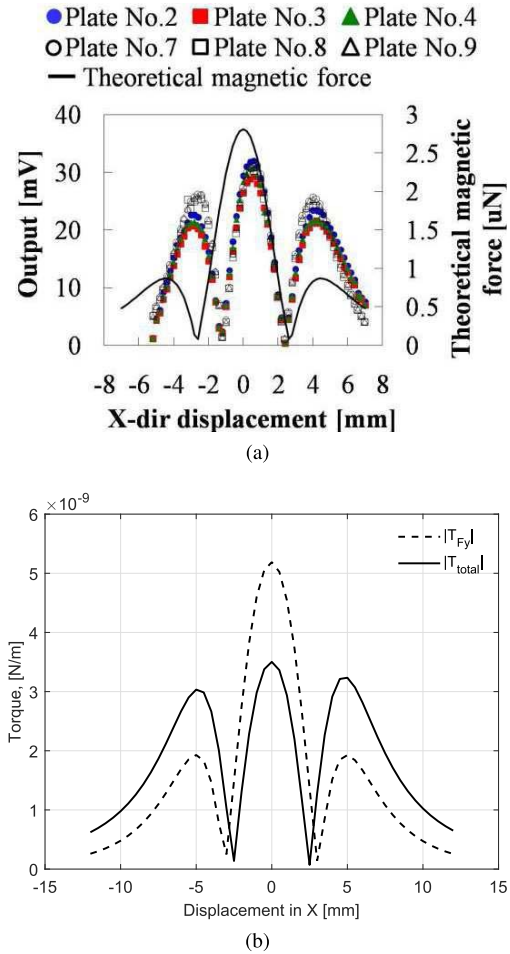


Fig. 8. (a) Output voltage from Wang’s piezoelectric transducer versus its lateral position relative to a zip-cord [16]. (b) Analytic result comparing the torque on a cantilever resulting from the vertical force alone,  $\tau(F_y)$ , (dashed line) versus the total torque,  $\tau_{total}$ , for a zip-cord.

different to results reported by Leland *et al.* [7] for his current sensor. Leland’s results are reasonably well matched to the theoretical curves for  $F_y$  and the influence of  $\tau_{mag}$  appears to have a negligible impact on the shape of the sensor output versus location (although it may well explain the asymmetry observed for both the single and two wire measurements). The discrepancy between Leland’s results and those reported here could be attributed to the small size and shape of the magnet. Leland’s magnets were deposited by applying a droplet of adhesive using a direct write printer to the tip of a silicon cantilever. Magnetic powder was then manually dispersed over the MEMS die and adhered itself to the epoxy droplet. The process was repeated until a dome with a base diameter of  $150 \mu\text{m}$  and  $100 \mu\text{m}$  tall, with alternating layers of epoxy and magnetic particles was achieved. It is beyond the scope of this paper to model this complex magnet geometry but we suggest that the semi-hemispherical shape of the printed magnet explains why  $\tau_{mag}$  had a negligible impact on Leland’s measured results.

Consider the magnetic torque acting on a discretized rectangular or cylindrical magnet as shown in Figure 9. The magnetic torque on each element of the magnet can be resolved into a net force couple, acting at the top and bottom of the element.

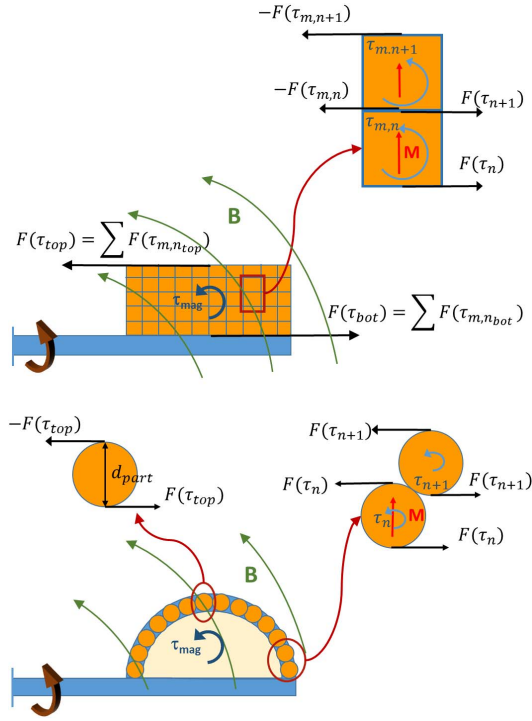


Fig. 9. Schematic showing a discretized rectangular magnet on cantilever beam (top) and a dome shaped magnet comprising magnetic particles adhered to a printed epoxy dome (bottom).

These forces cancel each other within the body of the magnet, leaving a net force that acts along the top of the magnet and an equal force acting along the bottom surface of the magnet. Assuming a very thin beam, only the force at the top of the magnet contributes to the equivalent magnetic torque at the anchor, where  $\tau_{mag} = F(\tau_{top}) \cdot d_{mag}$ . In the case of a dome shaped magnet, a similar effect can be assumed for magnetic particles piled on top of each other on Leland's epoxy dome. For those magnetic particles located towards the top of the dome, it can be shown that their contribution is much smaller than for the flat-topped magnet. This is because the contribution to the torque at the anchor resulting from the force couple on a single magnetic particle at the top of the dome is approximately equal to  $F(\tau_{top}) \cdot d_{part}$  where  $d_{part}$  is the height of the magnetic particle. Since  $d_{part} \ll d_{mag}$  the resulting torque at the anchor is therefore minimal compared with a flat-topped magnet.

## V. CONCLUSIONS

The location dependence of an electromagnetic transducer with respect to its source, an AC power line, is analyzed. The transducer is a silicon based MEMS cantilever with an integrated piezoelectric layer and with a permanent magnet disposed along its length. Placed in proximity to an AC current source, the cantilever oscillates with a frequency equal to that of the source and an electrical signal is generated across the piezoelectric capacitor. The position of the transducer with respect to the AC conductor is optimized here in order to maximize the tip displacement of the cantilever and consequently, the electrical output signal. Compared with previous work, where only the vertical component of the electromagnetic

force is considered, here the horizontal component of the force and the magnetic torque are also considered. It is found that the magnetic torque in particular is a very significant driver of the cantilever oscillations and cannot be neglected. This was found to be true both in the case of single wire and two wire sources.

## REFERENCES

- [1] W. He *et al.*, "Piezoelectric energy harvester scavenging AC magnetic field energy from electric power lines," *Sens. Actuators A, Phys.*, vol. 193, pp. 59–68, Apr. 2013.
- [2] R. Houlihan, O. Olszewski, F. Waldron, M. O'Neill, A. Mathewson, and N. Jackson, "Location dependence of a MEMS electromagnetic transducer with respect to an AC power source," *J. Phys., Conf. Ser.*, vol. 757, no. 1, p. 012041, 2016.
- [3] K. Isagawa, D. F. Wang, T. Kobayashi, T. Itoh, and R. Maeda, "Development of a MEMS DC electric current sensor applicable to two-wire electrical appliance cord," in *Proc. 6th IEEE Int. Conf. Nano/Micro Eng. Molecular Syst.*, Feb. 2011, pp. 932–935.
- [4] H. E. Knoepfel, *Magnetic Fields: A Comprehensive Theoretical Treatise for Practical Use*. Hoboken, NJ, USA: Wiley, 2008.
- [5] S. B. Lao, S. S. Chauhan, T. E. Pollock, T. Schröder, I. S. Cho, and A. Salehian, "Design, fabrication and temperature sensitivity testing of a miniature piezoelectric-based sensor for current measurements," *Actuators*, vol. 3, no. 3, pp. 162–181, 2014.
- [6] E. S. Leland, C. T. Sherman, P. Minor, P. K. Wright, and R. M. White, "A self-powered MEMS sensor for AC electric current," in *Proc. PowerMEMS*, 2009, pp. 53–56.
- [7] E. S. Leland, C. T. Sherman, P. Minor, P. K. Wright, and R. M. White, "A new MEMS sensor for AC electric current," in *Proc. SENSORS*, Nov. 2010, pp. 1177–1182.
- [8] E. S. Leland, R. M. White, and P. K. Wright, "Energy scavenging power sources for household electrical monitoring," in *Proc. PowerMEMS*, 2006, pp. 165–168.
- [9] E. S. Leland, P. K. Wright, and R. M. White, "A MEMS AC current sensor for residential and commercial electricity end-use monitoring," *J. Micromech. Microeng.*, vol. 19, no. 9, p. 094018, 2009.
- [10] D.-S. Nguyen, Z. Wu, and R. White, "Energy harvester for use on nearby current-carrying conductors," *J. Phys., Conf. Ser.*, vol. 660, no. 1, p. 012139, 2015.
- [11] O. Z. Olszewski, R. Houlihan, A. Blake, A. Mathewson, and N. Jackson, "Evaluation of vibrational piezoMEMS harvester that scavenges energy from a magnetic field surrounding an AC current-carrying wire," *J. Microelectromech. Syst.*, vol. 26, no. 6, pp. 1298–1305, Dec. 2017.
- [12] O. Z. Olszewski *et al.*, "A MEMS silicon-based piezoelectric AC current sensor," *Procedia Eng.*, vol. 87, pp. 1457–1460, 2014. [Online]. Available: <https://www.sciencedirect.com/science/article/pii/S187770581402846X>
- [13] I. Paprotny, Q. Xu, W. W. Chan, R. M. White, and P. K. Wright, "Electromechanical energy scavenging from current-carrying conductors," *IEEE Sensors J.*, vol. 13, no. 1, pp. 190–201, Jan. 2013.
- [14] Y. Suzuki, D. F. Wang, T. Kobayashi, Y. Suwa, T. Itoh, and R. Maeda, "Developing MEMS DC electric current sensor for end-use monitoring of DC power supply: Part III—Integration with actuating and sensing elements," in *Proc. Symp. Design, Test, Integr. Packag. MEMS/MOEMS (DTIP)*, Apr. 2013, pp. 1–4.
- [15] D. F. Wang *et al.*, "Passive MEMS DC electric current sensor: Part I—Theoretical considerations," *IEEE Sensors J.*, vol. 17, no. 5, pp. 1230–1237, Mar. 2017.
- [16] D. F. Wang *et al.*, "Passive MEMS DC electric current sensor: Part II—Experimental verifications," *IEEE Sensors J.*, vol. 17, no. 5, pp. 1238–1245, Jan. 2017.
- [17] W. Xian, X. Li, D. F. Wang, T. Kobayashi, T. Itoh, and R. Maeda, "Precise current sensing using a piezoelectric cantilever based current sensor," in *Proc. 19th Int. Conf. Solid-State Sens., Actuators Microsyst. (TRANSDUCERS)*, Jun. 2017, pp. 1057–1060.
- [18] W. Xian, D. F. Wang, D. F. Wang, T. Kobayashi, R. Maeda, and T. Itoh, "A passive position- and pose-free current sensor," in *Proc. IEEE 12th Int. Conf. Nano/Micro Eng. Mol. Syst. (NEMS)*, Apr. 2017, pp. 29–33.
- [19] W. Xian and D. F. Wang, "Position and orientation correction scheme for current sensing based on magnetic piezoelectric cantilevers," *Appl. Phys. Lett.*, vol. 110, no. 14, p. 143501, 2017.
- [20] Q. R. Xu, I. Paprotny, M. Seidel, R. M. White, and P. K. Wright, "Stick-on piezoelectromagnetic AC current monitoring of circuit breaker panels," *IEEE Sensors J.*, vol. 13, no. 3, pp. 1055–1064, Mar. 2013.



**Ruth Houlihan** received the bachelor's degree in mechanical engineering from the National University of Ireland, Galway, in 1998, the master's degree in engineering science from the University College Cork, Ireland, in 2000, and the Ph.D. degree in micromechanical systems from the University of Southampton, U.K., in 2004. She is currently a Staff Research Scientist with the Tyndall National Institute, Ireland. She was involved in inertial MEMS, RF MEMS, and energy harvesting devices as a device designer, process developer, modeler, and a test engineer. He was also involved in European projects and industrial contracts. In particular, she has focused on finite element and system level modeling of MEMS and on the test and analysis of reliability of MEMS. She has been the PI for Enterprise Ireland and ESA-funded projects.

**Nathan Jackson** (SM'14) received the B.S.E. (*summa cum laude*), M.S., and Ph.D. degrees in bioengineering from Arizona State University, USA, in 2003, in 2008, and in 2009, respectively. He then worked as a Senior Research Scientist with the Micro Nano System Centre, Tyndall National Institute, Cork, Ireland. He is currently an Assistant Professor with the Mechanical Engineering Department, The University of New Mexico, where he is also a member of the Center for High Technology Materials. His research interests include: piezoelectrics, smart materials, MEMS, energy harvesters, acoustic resonators, BioMEMS, and flexible/stretchable circuits.

Dr. Jackson is a Senior Member of the IEEE and the IEEE Engineering in Medicine and Biology Society.

**Alan Mathewson** (M'90–SM'98) received the B.Sc. degree in electrical engineering from the University of Newcastle, Newcastle upon Tyne, U.K., in 1978, and the Ph.D. degree in avalanche photodiode arrays compatible with complementary metal oxide semiconductor from University College Cork, Cork, Ireland. He is currently the Deputy Head of circuits and systems, Micro Nano Systems Centre, Tyndall National Institute. He has authored or coauthored of over 300 publications in peer-reviewed specialty journals and conference proceedings. He is a Senior Member of the IEEE.

**Oskar Z. Olszewski** received the B.Sc. degree in electronics from the Gdynia Maritime Academy, Gdynia, Poland, in 2002, the M.Eng. degree in electronic engineering from the Cork Institute of Technology, Cork, Ireland, in 2004, and the Ph.D. degree in microelectronics from University College Cork, Cork, in 2010. He is currently a Research Engineer with the Tyndall National Institute, Cork, where he is currently involved in research in the field of MEMS technology. His interests include device design and modeling, process development, and device characterization. In particular, he currently involves in piezoelectric resonators, energy harvesters, micropumps, aerosol generators, and MEMS switches.